Direct *ab Initio* Dynamics Calculations of Thermal Rate Constants and Kinetic Isotope Effects for the H + H_2O ↔ OH + H_2 Reaction

Thanh N. Truong* and Tom J. Evans

Department of Chemistry, University of Utah, Salt Lake City, Utah 84112

Received: May 6, 1994; In Final Form: June 28, 1994⊗

We present an application of our previously proposed direct *ab initio* dynamics method for calculating the thermal rate constants and kinetic isotope effects (KIEs) of the H + H_2O ↔ OH + H_2 reaction. Dynamical calculations were based on a full canonical variational transition-state theory plus multidimensional semiclassical tunneling corrections. The minimum energy path (MEP) and Hessians at selected points along this path were calculated at the QCISD/6-311+G(d,p) level of theory. The classical potential energy along the MEP was further improved by a series of single-point PMP4/6-311++G(2df,2pd) calculations. The predicted rate constants and KIEs are in excellent agreement with experimental data for the temperature range from 250 to 2000 K. The accuracy of the Schatz−Elgersma analytical potential energy function for this reaction has also been examined.

I. Introduction

The forward and reverse reactions

$$H + H_2O \leftrightarrow OH + H_2 \qquad (R1)$$

are of considerable importance in combustion chemistry. Experimentally, there are several measurements of thermal rate constants for both the forward[1,2] and reverse[3−8] reactions. Furthermore, recent advances in dynamics experiments have shown that reaction R1 exhibits state-specific and bond-specific rate enhancements.[9−18] These results have attracted significant interest in the theoretical chemical physics community, with several reaction dynamics studies[19−41] being reported. All of these studies, either quantum or semiclassical calculations, were based on the analytical global Schatz−Elgersma potential energy function[42] (PEF) which was fitted to POL-CI calculations by Walch and Dunning.[43] There we used the term "potential energy function" to indicate that it is an analytical function which was fitted to a Born−Oppenheimer potential energy surface. Previous full canonical variational transition-state theory (CVT) plus multidimensional small-curvature semiclassical adiabatic ground-state (SCSAG) tunneling calculations[33] using this PEF yielded thermal rate constants that are noticeably larger than the experimental reverse rate constants measured by Michael and Sutherland[2] in the low-temperature range. This discrepancy has been ascribed to the barrier width of the Schatz−Elgersma PEF being too thin.[2] Recent quantum calculations[38,44] using the Schatz−Elgerma PEF also yield the thermal rate constants for the OH + H_2 reaction being too large, in particular at low temperatures. Thus, it is of importance to perform accurate *ab initio* rate calculations for the above reactions to verify the accuracy of the Schatz−Elgersma PEF.

In our previous studies, we have proposed new "direct *ab initio* dynamics" methods for calculating thermal rate constants and related observables such as kinetic isotope effects for gas-phase chemical reactions from *first principles*.[45−46] In this approach, the potential energy surface information required for the dynamical calculations can be calculated at a sufficiently accurate level of *ab initio* electronic structure theory or density functional theory. The dynamical theory is based on a full canonical variational transition-state theory (CVT) which can account for the recrossing effects by including both the entropic and enthalpic effects in locating the optimal dynamical bottleneck along the minimum energy path (MEP). Furthermore, quantum mechanical tunneling can also be included quantitatively without much additional computational effort by using the multidimensional centrifugal-dominant small-curvature semiclassical adiabatic ground-state tunneling (SCT) method. We have applied these new methods to the hydrogen-abstraction H + CH_4 ↔ CH_3 + H_2 reaction and were able to *predict* both the forward and reverse thermal rates with excellent agreement with experimental data for a wide range of temperatures.[45,46] Although the results were quite encouraging, further applications and testing of the new methods are certainly needed to establish their range of applicability as well as their accuracy.

In this study, we have applied the above direct *ab initio* dynamics method for calculating the thermal rate constants of the H + H_2O ↔ OH + H_2 reaction. In these calculations, the potential energy surface was calculated at the quadratic configuration interaction including the single- and double-excitation (QCISD) levels of theory[47] using the 6-311+G(d,p) basis set with perturbative correction for the electron correlation energy along the minimum energy path at the PMP4/6-311++G(2df,-2pd) level added. The results from these calculations were then compared with the experimental data and CVT/SCT results using the Schatz−Elgersma PEF.

The paper is organized as follow. In section II, a brief overview of the CVT/SCT method used in this study is given. Computational details for both dynamical and electronic structure calculations are discussed in section III. Results and discussion are presented in section IV. Finally, conclusions are given in section V.

II. Dynamical Theory

A. Variational Transition-State Theory. Variational transition-state theory is based on the idea that by varying the dividing surface along a reference path to minimize the rate, one can minimize the error due to "recrossing" trajectories. In the present study, the reference path is the minimum energy path (MEP), which is defined as the steepest descent path from the saddle point to both the reactant and the product directions in the mass-weighted Cartesian coordinate system. The reaction

* Author to whom all correspondence should be addressed.
⊗ Abstract published in *Advance ACS Abstracts,* August 15, 1994.

0022-3654/94/2098-9558$04.50/0

coordinate s is then defined as the distance along the MEP with the origin located at the saddle point and is positive on the product side and negative on the reactant side. For a canonical ensemble at a given temperature T, the CVT rate constant for a bimolecular reaction is given by[48-54]

$$\kappa^{CVT}(T) = \min_s \kappa^{GT}(T,s) \tag{1}$$

where

$$\kappa^{GT}(T,s) = \frac{\sigma Q^{GT}(T,s)}{\beta h \Phi^R(T)} e^{-\beta V_{MEP}(s)} \tag{2}$$

In these equations, $k^{GT}(T,s)$ is the generalized transition-state theory rate constant at the dividing surface which intersects the MEP at s and is orthogonal to the MEP at the intersection point. σ is the symmetry factor accounting for the possibility of more than one symmetry-related reaction path. For the H_2O + H ↔ OH + H_2 reaction, σ equals 2 for both the forward and the reverse directions. β is $(k_bT)^{-1}$ where k_b is the Boltzmann constant; h is Planck's constant. $\Phi^R(T)$ is the reactant partition function (per unit volume for bimolecular reactions). $V_{MEP}(s)$ is the classical potential energy (also called the Born–Oppenheimer potential) along the MEP with its zero of energy at the reactants, and $Q^{GT}(T,s)$ is the internal partition function of the generalized transition state at s with the local zero of energy at $V_{MEP}(s)$. Both $\Phi^R(T)$ and $Q^{GT}(T,s)$ partition functions are approximated as the products of electronic, vibrational, and rotational partition functions. For the electronic partition function, the generalized transition-state electronic excitation energies and degeneracies are assumed to be the same as at the transition state. For the reaction studied here, we assume that there are no low-lying electronic excited states at the saddle point. For the OH radical, both $^2\Pi_{3/2}$ and $^2\Pi_{1/2}$ states were included, with the latter being 140 cm^{-1} higher in energy. For rotations, since the rotational energy levels are generally closely spaced, little accuracy is lost if we approximate the quantal rotational partition functions by the classical ones. For vibrations, in the present study, the partition functions are calculated quantum mechanically within the framework of the harmonic approximation. Thus, canonical variational transition-state theory yields the hybrid (i.e., classical reaction path motion with other degrees of freedom quantized) rate constants. Furthermore, if the generalized transition state is located at the saddle point ($s = 0$), eq 2 reduces to the conventional transition-state theory.

To include quantal effects for motion along the reaction coordinate, we multiply CVT rare constants by a ground-state transmission coefficient, $\kappa^{CVT/G}(T)$. Thus, the final rate constant is

$$\kappa^{CVT/G}(T) = \kappa^{CVT/G}(T)\kappa^{CVT}(T) \tag{3}$$

B. Multidimensional Semiclassical Tunneling Methods. First, we approximate the effective potential for tunneling to be the vibrationally adiabatic ground-state potential curve defined by

$$V_a^G(s) = V_{MEP}(s) + \epsilon_{int}^G(s) \tag{4}$$

where $\epsilon_{int}^G(s)$ denotes the zero-point energy in vibrational modes transverse to the MEP. The ground-state transmission coefficient, $\kappa^{CVT/G}(T)$, is then approximated as the ratio of the thermally averaged multidimensional semiclassical ground-state transmission probability, $P^G(E)$, for reaction in the ground state to the thermally averaged classical transmission probability for one-dimensional scattering by the ground-state effective potential, $V_a^G(s)$.[50-60] If we denote the CVT transition state for temperature T as $s_*^{CVT}(T)$, the value of $V_a^G\{s_*^{CVT}(T)\}$, denoted as $E_*(T)$, is the quasiclassical ground-state threshold energy. Then

$$\kappa^{CVT/G}(T) = \frac{\int_0^\infty P^G(E) e^{-E/k_bT}\, dE}{\int_{E_*(T)}^\infty e^{-E/k_bT}\, dE} \tag{5}$$

Notice that the integral in the numerator of eq 5 involves E above $E_*(*(T)$, as well as tunneling energies below this. Thus, the semiclassical transmission probability, $P^G(E)$, accounts for both nonclassical reflection at energies above the quasiclassical threshold and nonclassical transmission, i.e., tunneling, at energies below that threshold. However, because of the Boltzmann factor in eq 5, tunneling is by far the more important of the two effects.

Several approximations for $P^G(E)$ are available; however, only two, namely, the zero-curvature[52] and the centrifugal-dominant small-curvature semiclassical adiabatic ground-state[59] approximations used in the present study, are briefly discussed here. For convenience, we labeled them ZCT and SCT for the zero-curvature tunneling and small-curvature tunneling cases, respectively.

The centrifugal-dominant small-curvature semiclassical adiabatic ground-state approximation (SCT) is a generalization of the Marcus–Coltrin approximation in which the tunneling path is distorted from the MEP out to a concave-side vibrational turning point in the direction of the internal centrifugal force. Instead of defining the tunneling path, the centrifugal effect is included by replacing the reduced mass by an effective reduced mass, $\mu_{eff}(s)$, which is used to evaluate imaginary action integrals and thereby tunneling probabilities. Note that in the mass-weighted Cartesian coordinate system, the reduced mass (μ) is set equal to 1 amu. The ground-state transmission probability at energy E is

$$P^G(E) = \frac{1}{1 + e^{-2\theta(E)}} \tag{6}$$

where $\theta(E)$ is the imaginary action interval evaluated along the tunneling path,

$$\theta(E) = \frac{2\pi}{h} \int_{s_l}^{s_r} [2\mu_{eff}(s)|E - V_a^G(s)|]^{1/2}\, ds \tag{7}$$

and where the integration limits, s_l and s_r, are the reaction-coordinate turning points defined by

$$V_a^G[s_l(E)] = V_a^G[s_r(E)] = E \tag{8}$$

Note that the ZCT results can be obtained by setting $\mu_{eff}(s)$ equal to μ in eq 7. The effect of the reaction-path curvature included in the effective reduced mass, $\mu_{eff}(s)$, is explained elsewhere.[59]

III. Computational Details

A. Electronic Structure Calculations. In our previous study,[45] we had found that the QCISD/6-311G(d,p) level of theory yields structural information and vibrational frequencies at both the equilibrium structure and transition state with an accuracy comparable to the more expensive CCSD(T)/cc–VQZ method for the CH_4 + H ↔ CH_3 + H_2 reaction. We also used the QCISD level of theory but with the bigger 6-311+G(d,p) basis in the present study. To improve the energetic information along the MEP as well as the heat of reaction, we have performed a series of single-point PMP4/6-311++G(2df,2pd) calculations at the Hessian grid points along the MEP and at the reactants and products.

The minimum energy path was calculated in the mass-weighted internal coordinates using the second-order Gonzalez

TABLE 1: Energies (hartree), Geometries (Bond Lengths in Å and Angles in deg), and Frequencies (cm^{-1}) for the H + H_2O ↔ OH + H_2 Reaction

species	energies QCISD[b]	energies MP4//QCISD[c]	geometries[a]	QCISD[b]	frequencies QCISD[b]	frequencies CCSD(T)[d]	frequencies exptl[e]
H	−0.499 818	−0.499 818					
H_2	−1.168340	−1.171739	r_{HH}	0.743(0.741)	4422	4409	4405
OH	−75.593285	−75.636249	r_{OH}	0.971(0.971)	3776	3729	3735
H_2O	−76.281552	−76.334136	r_{OH}	0.959(0.958)	3990	3938	3943
			$\angle_{HOH}$	103.6(104.5)	3887	3830	3832
					1655	1662	1648
H−H_2O_{TS}	−76.747421	−76.799302	r_{HO}	0.970(0.968)	3799	3741	
			$r_{OH'}$	1.308(1.329)	2370	2449	
			$r_{H'H''}$	0.836(0.829)	1103	1102	
			$\angle_{HOH'}$	97.2(97.1)	634	616	
			$\angle_{OH'H''}$	165.6(162.8)	546	403	
					1407*i*	1333*i*	

[a] For equilibrium structures, the values in parentheses are experimental data taken from ref 65; for the transition state, the values in parentheses are from previous CCSD(T)/cc−VQZ calculations done by Kraka et al.[64] [b] Using 6-311+G(d,p) basis set. [c] PMP4(SDTQ)/6-311++G(2df,2pd) energies at the QCISD/6-311+G(d,p) geometries. [d] From ref 64. [e] Experimental harmonic frequencies taken from ref 66.

and Schlegel[61] method with a step size of 0.04 $amu^{1/2}$ bohr. This method has been successfully applied in our previous direct *ab initio* dynamics studies[45,46] of the CH_4 + H ↔ CH_3 + H_2 reaction.

All electronic structure calculations were done by using the GAUSSIAN92 program.[62]

B. Variational Transition-State Theory and Semiclassical Tunneling Calculations. In this study, we employed the focusing technique presented in our previous study[45] to assure the convergence of the calculated rate constants with a minimal number of Hessian calculations. This was done by first carrying out the preliminary rate calculations with coarse Hessian grids to estimate the regions containing the temperature-dependent canonical transition states, $s_*^{CVT}(T)$, or having large reaction path curvature, where the "corner cutting" effect would also be large. The finer grids were then calculated for these critical regions to improve the accuracy of the calculated canonical rate constants and small-curvature tunneling probability. This approach allows us to obtain the optimal accuracy for a given computational resource.

The canonical transition state, i.e., the location of the maximum of the free energy of activation, for a given temperature was determined by a quadratic−quartic fit. Other computational details are the same as in our previous study.[45,46]

VTST and small-curvature tunneling calculations were done by using our new DiRate (Direct Rate) program.[63]

IV. Results and Discussions

A. Stationary Points. The total electronic energies, geometries, and vibrational frequencies of the equilibrium and transition-state structures are given in Table 1 along with the results from the previous CCSD(T) calculations[64] and available experimental data.[65,66] The geometries of H_2, OH, and H_2O calculated at the QCISD level agree very well with the experimental data and so as their calculated vibrational frequencies with the largest discrepancy of about 55 cm^{-1}. We also found that the QCISD/6-311+G(d,p) level yields comparable accuracy with the CCSD(T)/cc−VQZ method for predicting geometries and frequencies of the equilibrium structures. This is consistent with our earlier finding.[45] The QCISD transition state, however, is shifted in the reactant side relative to the CCSD(T) one. In particular, the QCISD active OH′ and H′H″ bonds are 1.308 and 0.836 Å as compared to the CCSD(T) values of 1.329 and 0.829 Å, respectively. Similar to our previous study, we found that the QCISD transition-state vibrational frequencies are quite similar to the CCSD(T) ones, though the latter require more computational resource.

TABLE 2: Reaction Energies and Classical Barrier Heights (kcal/mol) for the H + H_2O → OH + H_2 Reactio

level/basis	ΔE	ΔH_0^0	$\Delta V_f^\ddagger$	$\Delta V_r^\ddagger$
QCISD/6-311+G(d,p)	12.39	10.48	21.30	8.91
PMP4/6-311++G(2df,2pd)//QCISD	16.29	14.38	21.74	5.45
CCSD(T)/cc−pVQZ[a]	16.65	14.48	22.27	5.62
Schatz−Elgersma PEF[b]	15.20	12.89	21.29	6.09
exptl	16.64[c]	14.6 ± 0.14[d]		

[a] From ref 64. cc−pVQZ denotes the correlation consistent valence quadruple ζ plus polarizations, [5s4p3d2f1g/4s3p2d1f] basis. [b] From ref 33. [c] Back-calculated from experimental ΔH_0^0 (ref 67) and harmonic frequencies (taken from ref 66). [d] From ref 67.

It is also important to point out that the analytical Schatz−Elgersma PEF yields the transition-state structure to have the trans conformation, whereas previous POL-CI[43], CCSD(T),[64] and present QCISD calculations predicted it to have the cis structure. The dipole-induced−dipole interaction argument as pointed out earlier supports the cis structure.[64]

The heat of reaction and classical barrier heights are listed in Table 2. We found that the QCISD/6-311+G(d,p) level theory noticeably underestimates the reaction energy by an order of 4 kcal/mol, while it overestimates the classical barrier for the reverse OH + H_2 reaction by 3 kcal/mol as compared to the previous CCSD(T)/cc−pVQZ results. However, single-point PMP4/6-311++G(2df,2pd) calculations at the QCISD/6-311+G(d,p) optimized geometries, denoted as PMP4//QCISD for short, significantly improve the energetic results and yield comparable accuracy with the more expensive CCSD(T) calculations[64] with the difference of about 1 kcal/mol. The PMP4//QCISD reaction enthalpy at 0 K is also within the experimental error.[67] Also in comparison with the results from the CCSD(T)/cc−pVQZ calculations, the Schatz−Elgersma PEF predicts the smaller heat of reaction at 0 K by about 2 kcal/mol and the classical barriers within 1 kcal/mol difference.

In conclusion, we found that the QCISD/6-311+G(d,p) levels can provide accurate structural and frequency information, whereas additional single-point PMP4/6-311++G(2df,2pd) calculations at the QCISD geometries are needed to get accurate heats of reaction and barrier heights. This combination approach yields results comparable to the more expensive CCSD(T)/cc−pVQZ level of theory and was used to calculate thermal rate constants as presented below.

B. Minimum Energy Path. The geometries along the minimum energy path plotted vs the reaction coordinate are

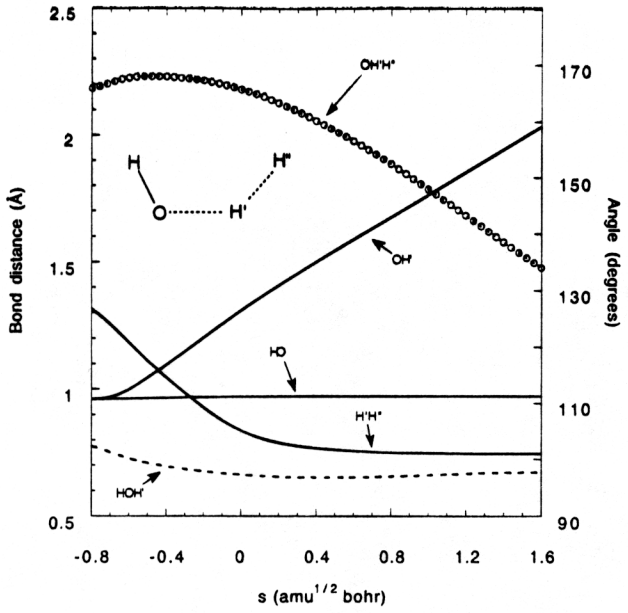

Figure 1. Geometries along the minimum energy path for the H + H_2 ↔ OH + H_2 reaction plotted vs the reaction coordinate s in the mass-weighted internal coordinates. Solid curves are bond distances (in Å) and dashed curves are angles (in deg). Small circles are calculated points along the MEP.

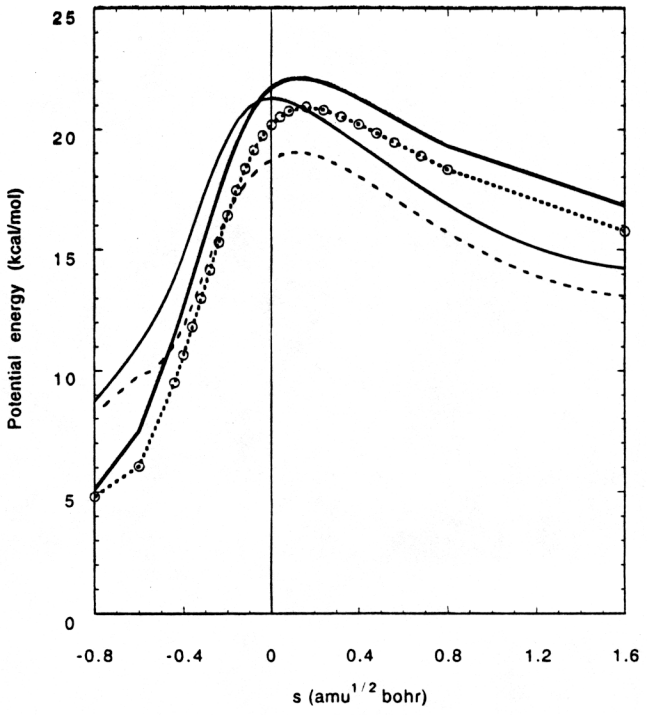

Figure 2. Classical potential $V_{MEP}(s)$ (solid curves) and ground-state vibrationally adiabatic potential $VF_a^G(s)$ (dashed curves) energies along the MEP as functions of the reaction coordinate s. Circles are points on the MEP where Hessian information is available. Thick lines are the present PMP4/6-311++G(2df,2pd)//QCISD/6-3111+G(d,p) results, and thin lines are from the Schatz−Elgersma PEF.

shown in Figure 1. Note that the formation of the HH bond in the forward direction is faster than the formation of the OH bond in the reverse direction. In particular, the formation of the H′H″ bond is about 93% completed at $s = 0.2$, whereas the formation of the OH′ bond is only 75% completed at $s = -0.2$. Furthermore, as the reaction proceeds toward the products, the angle OH′H″ decreases due to increasing importance of the dipole-induced−dipole interaction of the OH and H_2 molecules. As a technical point, the smooth changes in the internal coordinates along the reaction coordinate indicate the stability of the Gonzalez and Schlegel integration method.

The classical and zero-point energy corrected potential energy curves along the MEP calculated at the PMP4//QCISD level of theory are plotted in Figure 2 also with those from the analytical Schatz−Elgersma PEF. Recall s in the present calculation is defined as the distance along the QCISD MEP with the origin being at the saddle point. Notice that the PMP4//QCISD calculations shift the saddle point toward the product side slightly to the s value of about 0.16 and raise the classical barrier for the reverse reaction to 5.83 kcal/mol (see Figure 2). Since the QCISD transition state (i.e., at $s = 0.0$) is located on the reactant side relative to the CCSD(T) one, the PMP4 calculations in fact shift the QCISD MEP closer to the previous CCSD(T) results. Compared with the Schatz−Elgersma (SE) PEF, we found that the SE barrier width is narrower, and this is consistent with earlier suggestions.[2] The zero-point energy correction to the barrier was found to be about 1 kcal/mol larger in the SE PEF than in our present calculations.

Examining the generalized frequency plot as functions of reaction coordinate shown in Figure 3, we found that the present QCISD calculations and the SE PEF yield surprisingly similar results given the difficulty in designing and fitting an analytical PEF. Quantitatively, however, the SE H_2O asymmetric stretch and bending modes have a noticeably larger drop in the frequencies at the transition state than the corresponding QCISD modes. This has two important consequences. First, the SE PEF has a larger zero-point energy correction for the barrier as mentioned above. Second, this larger drop in the frequencies also indicates the SE PEF may overestimate the rate enhancement due the vibrational excitation of the water asymmetric

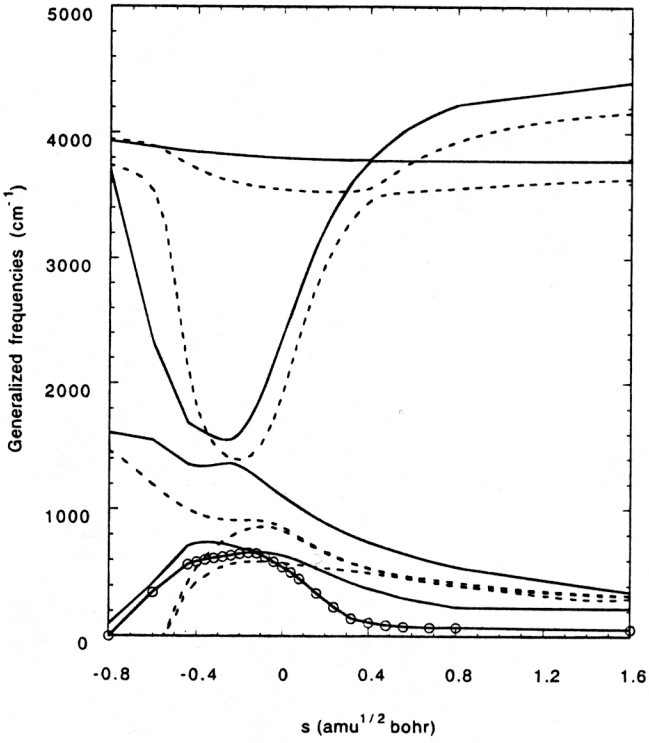

Figure 3. Harmonic vibrational frequencies along the reaction coordinate s. Solid curves are the QCISD/6-311+G(d,p) results, and dashed curves are from the Schatz−Elgersma PEF. Circles are points where QCISD Hessians were calculated.

stretch and bending modes. The latter is more relevant for understanding the mode-specific chemistry of the H + H_2O reaction. Since our present QCISD results agree much better with the more elaborate CCSD(T)/cc−pVQZ calculations[64] at the transition state, we would expect the present QCISD-generalized frequencies to be more accurate.

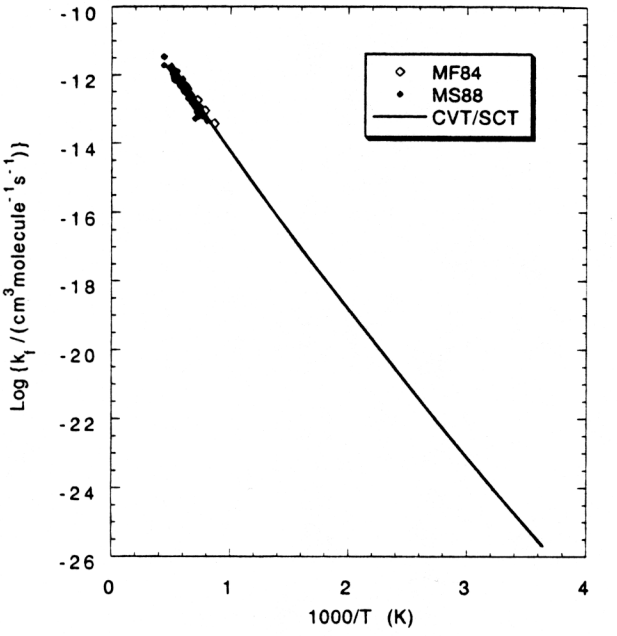

Figure 4. Arrhenius plot of the forward H + H_2O rate constants vs 1/*T*. The solid curve is the present CVT/SCT results. MF84, ref 1; MS88, ref 2.

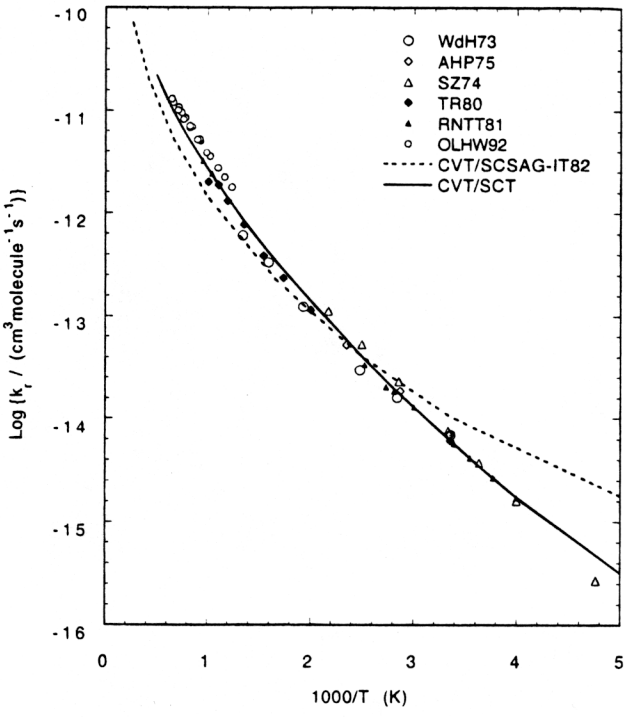

Figure 5. Arrhenius plot of the reverse OH + H_2 rate constants vs 1/*T*. The solid and dashed curves are from the present CVT/SCT results and previous CVT/SCSAG results (ref 33), respectively. WdH73, ref 5; AHP75, ref 6; SZ74, ref 4; TR80, ref 7; RNTT81, ref 3; OLHW92, ref 8.

C. Rate Constants. Canonical variational transition-state rate calculations augmented by the multidimensional centrifugal-dominant small-curvature semiclassical adiabatic ground-state tunneling corrections (CVT/SCT) were carried out for the range of temperatures from 250 to 2000 K. Due to the scattered Hessian information near the reactant and product regions, we restricted corner cutting effects only in the region within 3 kcal/mol from the maximum of the vibrationally ground-state adiabatic potential curve, i.e., the upper half of the barrier, in the SCT tunneling calculations. This corresponds to the energy with classical turning points within the ranges of [−0.14, 0.90] amu$^{1/2}$ bohr for the H + H_2O reaction (see Figure 2) and [−.20, 1.16] amu$^{1/2}$ bohr for the D + DOH → D_2 + OH reaction (see eq 8). For tunneling energy below this cutoff, the effect of the reaction path curvature on the tunneling probability is not included. Since tunneling probability is quite small in this energy range, the error from such a restriction for the temperature range considered in this study is expected to be small.

The Arrhenius plots of the calculated and experimental forward and reverse rate constants vs the temperatures are shown in Figures 4 and 5, respectively. Due to the substantial forward barrier, the experimental rate constants for the H + H_2O reaction are available only in the high-temperature region. The experimental rate constants for the OH + H_2 reaction, on the other hand, are available for a wider temperature range. Notice that our present CVT/SCT calculations predict rate constants in excellent agreement with the available experimental data for both forward and reverse reactions. In particular, the present *ab initio* results yield the curvature of the Arrhenius plot for the reverse rate constants in much better agreement with experimental data over the temperature range from 200 to 2000 K than the previous results[33] using Schatz−Elgersma PEF. The large curvature of the Arrhenius plot resulting from the tunneling contribution further indicates that the potential width of the Schatz−Elgersma PEF is too small.

Tables 3 and 4 list the rate constants calculated at different levels of approximations and the most recently recommended experimental values from the Arrhenius fit by Baulch et al.[68] for the forward and reverse reactions, respectively. Note the recommended forward rate coefficients were based on the scarce high-temperature measurements and rate data of the reverse reaction combined with the equilibrium constant.

TABLE 3: Calculated and Recommended Experimental Rate Constants (cm^3 molecule^{-1} s^{-1}) for the H + H_2 O → OH + H_2 Reaction[a]

T, K	TST	TST/W	CVT	CVT/ZCT	CVT/SCT	exptl[b]
250	1.90E-28	7.08E-28	5.47E-29	4.66E-28	6.87E-28	[4.06E-28]
300	1.61E-25	4.66E-25	6.15E-26	2.57E-25	3.62E-25	2.62E-25
350	2.02E-23	4.83E-23	9.47E-24	2.65E-23	3.52E-23	2.77E-23
400	7.70E-22	1.59E-21	4.22E-22	9.18E-22	1.16E-21	9.41E-22
500	1.31E-19	2.21E-19	9.21E-20	1.50E-19	1.76E-19	1.39E-19
600	4.23E-18	6.24E-18	3.33E-18	4.67E-18	5.25E-18	4.08E-18
700	5.25E-17	7.08E-17	4.50E-17	5.76E-17	6.29E-17	4.74E-17
800	3.58E-16	4.53E-16	3.27E-16	3.95E-16	4.22E-16	3.07E-16
1000	5.60E-15	6.55E-15	5.57E-15	6.28E-15	6.56E-15	4.46E-15
1200	3.73E-14	4.17E-14	3.73E-14	4.05E-14	4.18E-14	2.80E-14
1400	1.51E-13	1.64E-13	1.51E-13	1.61E-13	1.64E-13	1.08E-13
1600	4.47E-13	4.77E-13	4.47E-13	4.69E-13	4.77E-13	3.06E-13
2000	2.18E-12	2.28E-12	2.18E-12	2.25E-12	2.27E-12	1.39E-12

[a] The notation E-*n* stands for × 10^{-n} throughout. [b] Recommended values from Baulch et al.[68] Value in the square bracket is extrapolation.

For the forward H + H_2O reaction, the CVT/SCT rate constants are consistently larger than the recommended experimental values with the largest deviation factor of 1.63 at 2000 K. These factors are smaller at lower temperatures. Notice that the CVT/ZCT results, which do not include the "corner cutting" effect, yield noticeably better agreement with experimental data at temperatures below 1000 K. For example, at the room temperature of 300 K, the deviation factors are 0.96 and 1.27 for the CVT/ZCT and CVT/SCT methods, respectively. It is interesting to note that due to cancellation of errors in the recrossing and tunneling effects, the conventional TST with Wigner tunneling correction, TST/W, gives reasonable results, though about a factor of 2 too large compared to experimental data. To verify this, we have examined the CVT results, which include recrossing effects as well as additional electron correlation effects in the potential energy along the MEP but no tunneling, and found that they yield significantly smaller rate

TABLE 4: Calculated and Recommended Experimental Rate Constants (cm^3 $molecule^{-1}$ s^{-1}) for the OH + H_2 → H_2O Reaction

T, K	TST	TST/W	CVT	CVT/ZCT	CVT/SCT	exptl[a]
250	4.77E-16	1.78E-15	1.38E-16	1.17E-15	1.73E-15	[1.53E-15]
300	2.84E-15	8.22E-15	1.08E-15	4.55E-15	6.39E-15	6.18E-15
350	1.02E-14	2.43E-14	4.77E-15	1.33E-14	1.77E-14	1.74E-14
400	2.66E-14	5.51E-14	1.46E-14	3.18E-14	4.01E-14	3.90E-14
500	1.05E-13	1.77E-13	7.38E-14	1.20E-13	1.41E-13	1.28E-13
600	2.73E-13	4.02E-13	2.15E-13	3.01E-13	3.38E-13	2.98E-13
700	5.56E-13	7.49E-13	4.76E-13	6.10E-13	6.65E-13	5.66E-13
800	9.74E-13	1.23E-12	8.91E-13	1.08E-12	1.15E-12	9.42E-13
1000	2.28E-12	2.67E-12	2.27E-12	2.56E-12	2.68E-12	2.04E-12
1200	4.31E-12	4.83E-12	4.31E-12	4.69E-12	4.84E-12	3.60E-12
1400	7.15E-12	7.77E-12	7.15E-12	7.60E-12	7.78E-12	5.61E-12
1600	1.09E-11	1.16E-11	1.09E-11	1.14E-11	1.16E-11	8.06E-12
2000	2.12E-11	2.21E-11	2.12E-11	2.19E-11	2.21E-11	1.42E-11

[a] The notation E-*n* stands for × 10^{-n} throughout. [b] Recommended values from Baulch et al.[68] Value in the square bracket is extrapolation.

constants in the low-temperature range compared to the TST results. For example, at 300 K, the deviation factor k^{CVT}/k^{TST} is of the order 0.38. Such cancellation of errors had also been suggested in the previous TST/W calculation.[69]

For the reverse OH + H_2 reaction, similar observations were found except that the CVT/SCT calculations yield better agreement with experimental data, particularly at the lower temperature range. The calculated CVT/SCT rate constants are also slightly too large. The deviation factor is largest at 2000 K with the magnitude of 1.56 and decreases as the temperature decreases. At 300 K, it is only 1.03.

It is important to note that the harmonic approximation was used in the present CVT/SCT calculations. Anharmonicity had been found to lower the rate constants;[33] however, inclusion anharmonicity to our direct *ab initio* approach would require a substantial additional computation and, therefore, is not cost-effective at the present time.

In order to calculate the kinetic isotope effect as discussed below, we have also carried out rate calculations for the OH + D_2 reaction for the temperature range from 250 to 2000 K. The Arrhenius plot of the calculated and experimental rate constants[3] is shown in Figure 6. Notice that the present *ab initio* results give excellent agreement with the scarce experimental data for a wide range of temperatures; except for the temperature range of 500−1000 K, our calculated rate constants are somewhat smaller.

D. Kinetic Isotope Effects. The kinetic isotope effects for the reverse OH + H_2 reaction, k_{H_2}/k_{D_2}, as functions of temperature were calculated at different levels of approximation using the PMP4//QCISD potential surface and are given in Table 5 and also plotted in Figure 7. As mentioned in the previous study,[33] using the Schatz−Elgersma PEF in conjunction with the CVT/SCT method significantly overestimates the KIE, particularly in the low-temperature range as illustrated in Figure 7. This is partly due to the Schatz−Elgersma PEF potential width being too narrow as discussed above. By contrast, our present *ab initio* approach, namely, CVT/SCT, predicts the KIE within the experimental uncertainty[3] for temperatures below 300 K, but it is slightly too large for higher temperatures. Quantitatively, the largest percent error is about 53% at $T = 500$ K. Anharmonicity had been found to decrease the KIE;[33] thus, it would bring our predictions to better agreement with experimental observation. It is interesting to point out that the simple TST/W calculations also provide reasonably accurate KIE for the OH + H_2 reaction. By comparing the TST and CVT results, we found that recrossing and additional electron correlation can lower the KIE noticeably. Tunneling, on the other hand, tends to raise the KIE as expected. Thus, the good agreement with the experimental data resulted from cancellation of errors from the recrossing and tunneling effects in the TST/W method.

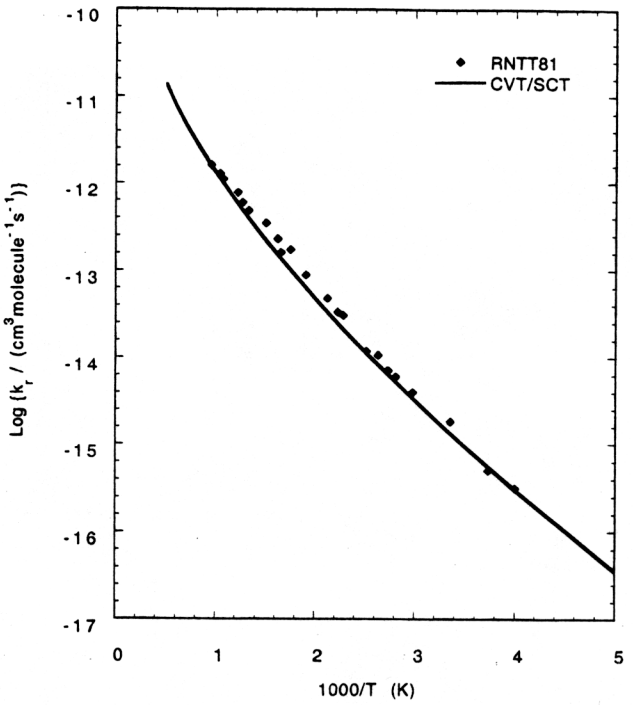

Figure 6. Arrhenius plot of the reverse OH + D_2 rate constants vs 1/*T*. The solid curve is from the present CVT/SCT results. RNTT81 is from ref 3.

TABLE 5: Calculated and Experimental Deuterium Kinetic Isotopc Effects (k_{H_2}/k_{D_2}) for the OH + H_2 → H_2O + H Reaction

T, K	TST	TST/W	CVT	CVT/ ZCT	CVT/ SCT	CVT/ SCT-SE[a]	exptl[b]
250	4.30	6.46	3.21	7.50	5.77	11.58	6.63
300	3.76	5.35	2.97	5.21	4.54	7.50	4.14
350	3.38	4.59	2.79	4.16	3.86	5.62	3.05
400	3.10	4.04	2.65	3.58	3.42	4.58	2.48
500	2.70	3.31	2.51	3.04	2.98	3.49	1.94
600	2.44	2.86	2.30	2.62	2.59	2.94	1.72
700	2.25	2.55	2.17	2.39	2.38	2.59	1.63
800	2.10	2.32	2.08	2.24	2.23	2.36	1.60
1000	1.90	2.04	1.94	2.03	2.03	2.05	1.63

[a] CVT/CD-SCSAG results (ref 33) using the Schatz−Elgersma PEF. [b] Calculated from Ravishankara et al.'s three-parameter functions (ref 3) for the measured rate constants.

V. Conclusions

We have applied our previously proposed direct *ab initio* dynamics method to calculate the thermal rate constants and kinetic isotope effects for the forward and reverse H + H_2O ↔ OH + H_2 reactions. The minimum energy path and Hessians at selected points along it were calculated by the QCISD/6-311+G(d,p) level of theory. Classical potential energy along the MEP was further improved by a series of single-point PMP4/6-311++G(2df,2pd) calculations.

We found that our proposed direct *ab initio* dynamics method was able to predict thermal rate constants for both the forward and reverse reactions as well as the kinetic isotope effects, in excellent agreement with the available experimental measurements for a wide range of temperatures, particularly from 250 to 2000 K. Our present results further confirm that the analytical Schatz−Elgersma PEF width is too narrow. We have also found that due to cancellation of errors in recrossing and tunneling effects, the simple TST plus Wigner tunneling corrections, which

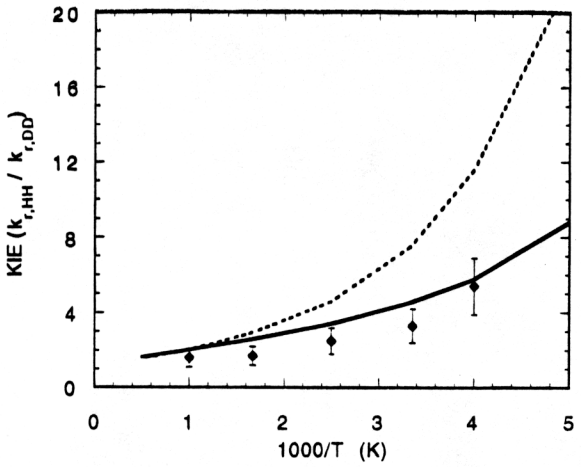

Figure 7. Kinetic isotope effects (k_{H_2}/k_{D_2}) for the OH + H2 reaction plotted vs 1000/*T* (K). The solid and dashed curves are the CVT/SCT results from the present *ab initio* surface and the Schatz–Elgersma PEF, respectively. Diamonds are experimental data from ref 3.

have often been used in conjunction with *ab initio* calculations to estimate rate constants, can yield reasonable rate constants and KIE.

This study has illustrated the versatility as well as the applicability of the direct *ab initio* dynamics method for predicting the kinetic properties of chemical reactions in the gas phase from first principles. Furthermore, it also provides potential energy information which can be used to examine or to further improve the accuracy of analytical PEF which is still quite useful for other types of dynamical calculations.

Acknowledgment. This work was supported by the National Science Foundation via an NSF Young Investigator Award to T.N.T. and by the University of Utah. We are grateful to the reviewers for their comments.

References and Notes

(1) Madronich, S.; Felder, W. *J. Phys. Chem.* **1984**, *88*, 1857.
(2) Michael, J. V.; Sutherland, J. W. *J. Phys. Chem.* **1988**, *92*, 3853.
(3) Ravishankara, A. R.; Nicovich, J. M.; Thompson, R. L.; Tully, F. P. *J. Phys. Chem.* **1981**, *85*, 2498.
(4) Smith, I. W. M.; Zellner, R. *J. Chem. Soc., Faraday Trans. 2* **1974**, *70*, 2290.
(5) Westenberg, A. A.; deHass N. *J. Chem. Phys.* **1973**, *58*, 4061.
(6) Atkinson, R.; Hansen, D. A.; Pitts, J. N. *J. Chem. Phys.* **1975**, *63*, 1703.
(7) Tully, F. P.; Ravishankara, A. R. *J. Phys. Chem.* **1980**, *84*, 3126.
(8) Oldenborg, R. C.; Loge, G. W.; Harradine, D. M.; Winn, K. R. *J. Phys. Chem.* **1992**, *96*, 8426.
(9) Sinha, A. *J. Phys. Chem.* **1990**, *94*, 4391.
(10) Adelman, D. E.; Filseth, S. V.; Zare, R. N. *J. Chem. Phys.* **1993**, *98*, 4636.
(11) Bronikowski, M. J.; Simpson, W. R.; Zare, R. N. *J. Phys. Chem.* **1993**, *97*, 2194.
(12) Bronikowski, M. J.; Simpson, W. R.; Zare, R. N. *J. Phys. Chem.* **1993**, *97*, 2204.
(13) Alagia, M.; Balucani, N.; Casavecchia, P.; Stranges, D.; Volpi, G. G. *J. Chem. Phys.* **1993**, *98*, 2459.
(14) Hsiao, M. C.; Sinha, A.; Crim, F. F. *J. Phys. Chem.* **1991**, *95*, 8263.
(15) Sinha, A.; Hsiao, M. C.; Crim, F. F. *J. Chem. Phys.* **1991**, *94*, 4928.
(16) Sinha, A.; Hsiao, M. C.; Crim, F. F. *J. Chem. Phys.* **1990**, *92*, 6333.
(17) Alagia, M.; Balucani, N.; Casavecchia, P.; Stranges, D.; Volpi, G. G. *J. Chem. Phys.* **1993**, *98*, 2459.
(18) Sinha, A. *J. Phys. Chem.* **1990**, *94*, 4391.
(19) Bowman, J. M.; Wang, D. S. *J. Chem. Phys.* **1992**, *96*, 7852.
(20) Wang, D. S.; Bowman, J. M. *Chem. Phys. Lett.* **1993**, *207*, 227.
(21) Wang, D. S.; Bowman, J. M. *J. Chem. Phys.* **1993**, *98*, 6235.
(22) Kudla, K.; Schatz, G. C. *J. Chem. Phys.* **1993**, *98*, 4644.
(23) Szichman, H.; Last, I.; Baram, A.; Baer, M. *J. Phys. Chem.* **1993**, *97*, 6436.
(24) Clary, D. C. *Chem. Phys. Lett.* **1992**, *192*, 34.
(25) Clary, D. C. *J. Chem. Phys.* **1992**, *96*, 3656.
(26) Clary, D. C. *J. Chem. Phys.* **1991**, *95*, 7298.
(27) Marcus, R. A. *J. Phys. Chem.* **1991**, *95*, 8236.
(28) Billing, G. D. *Chem. Phys.* **1990**, *146*, 63.
(29) Harrison, J. A.; Mayne, H. R. *J. Chem. Phys.* **1988**, *88*, 7424.
(30) Cohen, N.; Benson, S. W. *J. Phys. Chem.* **1987**, *91*, 162.
(31) Harrison, J. A.; Mayne, H. R. *J. Chem. Phys.* **1987**, *87*, 3689.
(32) Brown, N. J.; Rashed, O. *J. Chem. Phys.* **1986**, *85*, 4348.
(33) Isaacson, A. D.; Truhlar, D. G. *J. Chem. Phys.* **1982**, *76*, 1380.
(34) Wang, D.; Bowman, J. M. *J. Chem. Phys.* **1992**, *96*, 8906.
(35) Zhang, D. H.; Zhang, J. Z. H. *J. Chem. Phys.* **1993**, *99*, 5615.
(36) Echave, J.; Clary, D. C. *J. Chem. Phys.* **1994**, *100*, 402.
(37) Nyman, G.; Clary, D. C. *J. Chem. Phys.* **1993**, *99*, 7774.
(38) Manthe, U.; Seideman, T.; Miller, W. H. *J. Chem. Phys.* **1993**, *99*, 10078.
(39) Kudla, K.; Schatz, G. C. *J. Chem. Phys.* **1993**, *98*, 4644.
(40) Bradley, K. S.; Schatz, G. C. *J. Phys. Chem.* **1994**, *98*, 3788.
(41) Schatz, G. C.; Colton, M. C.; Grant, J. L. *J. Phys. Chem.* **1984**, *88*, 2971.
(42) Schatz, G. C.; Elgersma, H. *Chem. Phys. Lett.* **1980**, *73*, 21.
(43) Walch, S. P.; Dunning, T. H. *J. Chem. Phys.* **1980**, *72*, 1303.
(44) Bowman, J. M.; Wang, D. Unpublished results taken from ref 38.
(45) Truong, T. N. *J. Chem. Phys.* **1994**, *100*, 8014.
(46) Truong, T. N.; Duncan, W. T. *J. Chem. Phys.*, in press.
(47) Pople, J. A.; Head-Gordon, M.; Raghavachari, K. *J. Chem. Phys.* **1987**, *87*, 5968.
(48) Garrett, B. C.; Truhlar, D. G. *J. Chem. Phys.* **1979**, *70*, 1593.
(49) Truhlar, D. G.; Garrett, B. C. *Acc. Chem. Rev.* **1980**, *13*, 440.
(50) Truhlar, D. G.; Isaacson, A. D.; Skodje, R. T.; Garrett, B. C. *J. Phys. Chem.* **1982**, *86*, 2252.
(51) Truhlar, D. G.; Garrett, B. C. *Annu. Rev. Phys. Chem.* **1984**, *35*, 159.
(52) Truhlar, D. G.; Isaacson, A. D.; Garrett, B. C. In *Theory of Chemical Reaction Dynamics*; Baer, M., Ed.; CRC: Boca Raton, FL, 1985; Vol. 4, pp 65–137.
(53) Truhlar, D. G.; Garrett, B. C. *J. Chem. Phys.* **1987**, *84*, 365.
(54) Tucker, S. C.; Truhlar, D. G. In *New Theoretical Concepts for Understanding Organic Reactions*; Bertran, J., Csizmadia, I. G., Eds.; Kluwer: Dordrecht, The Netherlands, 1989; pp 291–346.
(55) Garrett, B. C.; Abushalbi, N.; Kouri, D. J.; Truhlar, D. G. *J. Chem. Phys.* **1985**, *83*, 2252.
(56) Kreevoy, M. M.; Ostovic, D.; Truhlar, D. G.; Garrett, B. C. *J. Phys. Chem.* **1986**, *90*, 3766.
(57) Isaacson, A. D.; Garrett, B. C.; Hancock, G. C.; Rai, S. N.; Redmon, M. J.; Steckler, R.; Truhlar, D. G. *Comput. Phys. Commun.* **1987**, *47*, 91.
(58) Garrett, B. C.; Joseph, T.; Truong, T. N.; Truhlar, D. G. *Chem. Phys.* **1989**, *136*, 271.
(59) Lu, D.-h.; Truong, T. N.; Melissas, V. S.; Lynch, G. C.; Liu, Y. P.; Garrett, B. C.; Steckler, R.; Isaacson, A. D.; Rai, S. N.; Hancock, G. C.; Lauderdale, J. G.; Joseph, T.; Truhlar, D. G. *Comput. Phys. Commun.* **1992**, *71*, 235.
(60) Liu, Y.-P.; Lu, D.-h.; Gonzalez-Lafont, A.; Truhlar, D. G.; Garrett, B. C. *J. Am. Chem. Soc.* **1993**, *115*, 7806.
(61) Gonzalez, C.; Schlegel, H. B. *J. Phys. Chem.* **1990**, *94*, 5523.
(62) Frisch, M. J.; Trucks, G. W.; Head-Gordon, M.; Gill, P. M. W.; Wong, M. W.; Foresman, J. B.; Johnson, B. G.; Schlegel, H. B.; Robb, M. A.; Replogle, E. S.; Gomperts, R.; Andres, J. L.; Raghavachari, K.; Binkley, J. S.; Gonzalez, C.; Martin, R. L.; Fox, D. J.; Defrees, D. J.; Baker, J.; Stewart, J. J. P.; Pople, J. A. *Gaussian 92*; Gaussian, Inc.: Pittsburgh, PA, 1992.
(63) Truong, T. N. *DiRate* (unpublished); University of Utah: Salt Lake City, 1993.
(64) Kraka, E.; Gauss, J.; Cremer, D. *J. Chem. Phys.* **1993**, *99*, 5306.
(65) Defrees, D. J.; Levi, B. A.; Pollack, S. K.; Hehre, W. J.; Binkley, J. S.; Pople, J. A. *J. Am. Chem. Soc.* **1979**, *101*, 4085.
(66) Jacox, M. E. *J. Phys. Chem. Ref. Data* **1990**, *19*, 387.
(67) Furue, H.; Pacey, P. D. *J. Phys. Chem.* **1990**, *94*, 1419.
(68) Baulch, D. L.; Cobos, C. J.; Cox, R. A.; Esser, C.; Frank, P.; Just, T.; Kerr, J. A.; Pilling, M. J.; Troe, J.; Walker, R. W.; Warnatz, J. *J. Phys. Chem. Ref. Data* **1992**, *21*, 441.
(69) Schatz, G. C.; Walch, S. P. *J. Chem. Phys.* **1980**, *72*, 776.